Deuteron electrodisintegration with unitarily evolved potentials

S. N. More, S. König, R. J. Furnstahl, and K. Hebeler

Deuteron electrodisintegration with unitarily evolved potentials

S. N. More,[1, *] S. König,[1, †] R. J. Furnstahl,[1, ‡] and K. Hebeler[2, 3, §]

[1]*Department of Physics, The Ohio State University, Columbus, Ohio 43210, USA*
[2]*Institut für Kernphysik, Technische Universität Darmstadt, 64289 Darmstadt, Germany*
[3]*ExtreMe Matter Institute EMMI, GSI Helmholtzzentrum für Schwerionenforschung GmbH, 64291 Darmstadt, Germany*

Renormalization group (RG) methods used to soften Hamiltonians for nuclear many-body calculations change the effective resolution of the interaction. For nucleon knock-out processes, these RG transformations leave cross sections invariant, but initial-state wave functions, interaction currents, and final-state interactions are individually altered. This has implications for the factorization of nuclear structure and reactions. We use deuteron electrodisintegration as a controlled laboratory for studying how structure and reaction components are modified under RG evolution, without the complication of three-body forces or currents. The dependence of these changes on kinematics is explored.

I. INTRODUCTION

Softened or "low momentum" interactions are widely used in contemporary nuclear structure calculations because they exhibit faster convergence for methods using basis expansions (this includes coupled cluster, configuration interaction, in-medium similarity renormalization group, and self-consistent Green's function methods) [1, 2]. Such interactions are derived using unitary transformations starting from chiral effective field theory or phenomenological interactions that exhibit significant coupling of high- and low-momentum physics. When done in small steps, these unitary transformations are a type of renormalization group (RG) transformation. The RG decoupling scale can be associated with the resolution of the interaction [2].

But how do we handle observables involving external probes when using such interactions? Nuclear structure has conventionally been treated as largely separate from nuclear reactions. However, this separation implies a unique factorization of experimental cross sections into the structure and reaction parts. The RG perspective informs us that such a division is itself inevitably resolution dependent [3]. In some circumstances the dependence is small and one can define the separation with negligible ambiguity. But the significant (and beneficial) changes to wave functions from evolving to lower resolution with RG methods imply significant changes to this separation. That is, what is structure at one resolution becomes part of the reaction mechanism at another resolution (and vice versa). This separation is not only scale dependent, it is *scheme* dependent as well; that is, it depends on *how* the separation is carried out and on the details of the original Hamiltonian.

* more.13@osu.edu
† koenig.389@osu.edu
‡ furnstahl.1@osu.edu
§ kai.hebeler@physik.tu-darmstadt.de

This observation raises questions of consistency and uniqueness in analyzing and interpreting nuclear experimental data. For example, it is clear from previous calculations using the similarity RG (or SRG) [1, 4, 5] that the high-momentum tail of the momentum distribution in a nucleus is dramatically resolution dependent for the range of decoupling scales used in present-day nuclear structure calculations. How then can such a distribution be said to be extracted from experiment? Yet it is common in the literature that high-momentum components are treated as measurable, at least implicitly [6–9]. In fact, what can be extracted is the momentum distribution at some scale, and with the specification of a scheme. This makes momentum distributions model dependent [10, 11].

This is relevant for recent work to extract a "nuclear contact" [12–14]. For some physical systems under certain conditions, such as the high-momentum $1/k^4$ tail in cold atoms at unitarity [15], the scale and scheme dependence is negligible, so it *can* be determined essentially uniquely. But for nuclei this dependence may be substantial and one needs to carefully define the short-distance content of the nuclear contact. As illustrated in [16], the nuclear shell structure is not a measurable. Its extraction from experimental data involves fixing a scale and a scheme.

In general, to be consistent between structure and reactions one must calculate cross sections or decay rates within a single framework. That is, one must use the same Hamiltonian and consistent operators throughout the calculation (which means the same scale and scheme). Such consistent calculations have existed for some time for few-body nuclei (e.g., see [17–20]) and are becoming increasingly feasible for heavier nuclei because of advances in reaction technology, such as using complex basis states to handle continuum physics. Recent examples in the literature include NCSM/RGM [21], coupled cluster [22], and lattice EFT calculations [23]. But there are many open questions about constructing consistent currents and how to compare results from two such calculations. Some work along this direction was done in

[24, 25] where the mean values for eigenstates of renormalized Hamiltonians were calculated using evolved operators. We seek to extend this to transition matrix elements and explore the connection to high-momentum physics in a nucleus in a controlled manner.

In particular, we will take the first steps in exploring the interplay of structure and reaction as a function of kinematic variables and SRG decoupling scale λ in a controlled calculation of a knock-out process. There are various complications for such processes. With RG evolution, a Hamiltonian—even with only a two-body potential initially—will develop many-body components as the decoupling scale decreases. Similarly, a one-body current will develop two- and higher-body components.

Our strategy is to avoid dealing with all of these complications simultaneously by considering the cleanest knock-out process: deuteron electrodisintegration with only an initial one-body current. With a two-body system, there are no three-body forces or three-body currents to contend with. Yet it still includes several key ingredients to investigate: i) the wave function will evolve with changes in resolution; ii) at the same time, the one-body current develops two-body components, which are simply managed; and iii) there are final-state interactions (FSI). It is these ingredients that will mix under the RG evolution. We can focus on different effects or isolate parts of the wave function by choice of kinematics. For example, we can examine when the impulse approximation is best and to what extent that is a resolution-dependent assessment.

We will vary the interaction resolution using SRG transformations, which have proven to be technically feasible for evolving three-body forces [26–29]. The SRG series of unitary transformations ensures that cross sections are invariant under changes in resolution. As the SRG λ is varied, the Hamiltonian $H(\lambda)$ and the nuclear wave function change, the current operator changes, and the FSI change as well. The question we address is: How do these combine to achieve the invariance of the observable cross section?

The electron scattering knock-out process is particularly interesting because of the connection to past, present, and planned experiments [30, 31]. The conditions for clean factorization of structure and reactions in this context is closely related to the impact of 3N forces, two-body currents, and final-state interactions, which have not been cleanly understood as yet [3]. All of this becomes particularly relevant for high-momentum-transfer electron scattering.[1] This physics is conventionally explained in terms of short-range correlation (SRC) phenomenology [6, 32]. SRCs are two- or higher-body components of the nuclear wave function with high

relative momentum and low center-of-mass momentum. These explanations would seem to present a puzzle for descriptions of nuclei with low-momentum Hamiltonians, for which SRCs are essentially absent from the wave functions.

This puzzle is resolved by the unitary transformations that mandate the invariance of cross section. The physics that was described by SRCs in the wave functions must shift to a different component, such as a two-body contribution from the current. This may appear to complicate the reaction problem just as we have simplified the structure part, but past work and analogies to other processes suggests that factorization may in fact become cleaner [4, 33]. One of our goals is to elucidate this issue, although we will only start to do so in the present work.

The underlying picture is analogous to that used in deep inelastic scattering (DIS) [3, 5]. In the analysis of DIS, one introduces both a renormalization and a factorization scale. In the usual dimensional regularization minimal subtraction scheme $\overline{\text{MS}}$, the renormalization scale μ_R sets the division between long- and short-distance physics in the Hamiltonian. This is manifested in the running coupling $\alpha_s(\mu)$ where the choice of $\mu = \mu_R$ is to optimize the efficacy of the QCD perturbation expansion. The factorization scale μ_F dictates the division between what goes into the reaction part, namely the purely hard process described in pQCD, and the structure part, which is subsumed into the soft parton distribution functions. Changing μ_F changes the balance. In many cases these two scales are chosen to be the same and equal to the magnitude of the four-momentum transfer Q, in order to minimize the contribution of logarithms that can disturb the perturbative expansion.

The nuclear analogs to these two scales are tied together in the SRG evolution. In particular, the decoupling scale, roughly given by the value of the SRG flow parameter λ, sets both these scales. For the Hamiltonian, this scale clearly sets the division between low and high momentum. For operators acting on wave functions, the decoupling dictates the division between the two; e.g., the scale at which a one-body current is largely replaced by a two-body current. In the present paper, we will illustrate the combined interplay with quantitative calculations. We build upon previous work by Anderson *et al.* on SRG operator evolution for the deuteron [4], and the work by Yang and Phillips [34] in applying chiral EFT to deuteron electrodisintegration.

This paper is organized as follows. In Sec. II, we briefly review the electrodisintegration formalism and develop the machinery we need for the SRG evolution, which we accomplish in practice by appropriate insertions of unitary transformation matrices. In Sec. III, we present proof-of-principle tests and illustrate the interplay of the different components that enter in the calculation of the disintegration process. We give representative results for selected kinematics. In Sec. IV, we summarize our observations and plans to extend the calculations to other kinematics, as well as beyond the deuteron system and

---

[1] Note that high-momentum transfers imply high-resolution *probes*, which is different from the resolution induced by the RG transformation decoupling scale. How the latter should be chosen to best accommodate the former is a key unanswered question.

one-body initial currents.

II. FORMALISM

A. Deuteron electrodisintegration: a primer

Deuteron electrodisintegration is the simplest nucleon-knockout process and has been considered as a test ground for various NN models for a long time (see, for example, Refs. [9, 35]). It has also been well studied experimentally [36, 37]. As outlined in the introduction, the absence of three-body currents and forces makes it an ideal starting point for studying the interplay with SRG evolution of the deuteron wave function, current, and final-state interactions.

We follow the approach of Ref. [34], which we briefly review. The kinematics for the process in the laboratory frame is shown in Fig. 1. The virtual photon from
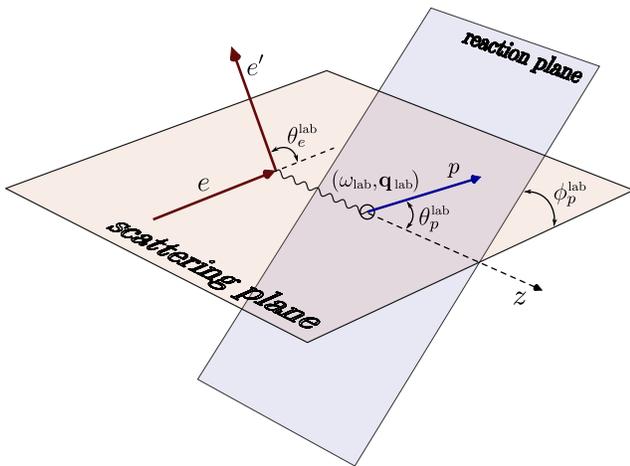

Figure 1. (color online) The geometry of the electrodisintegration process in the lab frame. The virtual photon disassociates the deuteron into the proton and the neutron (not shown in this figure).

electron scattering transfers enough energy and momentum to break up the deuteron into a proton and neutron. The differential cross section for deuteron electrodisintegration for unpolarized scattering in the lab frame is given by [38]

$$\frac{\mathrm{d}^3\sigma}{\mathrm{d}k'^{\mathrm{lab}}\mathrm{d}\Omega_e^{\mathrm{lab}}\mathrm{d}\Omega_p^{\mathrm{lab}}} = \frac{\alpha}{6\,\pi^2}\frac{k'^{\mathrm{lab}}}{k^{\mathrm{lab}}(Q^2)^2}\Big[v_L f_L + v_T f_T$$
$$+ v_{TT} f_{TT} \cos 2\phi_p^{\mathrm{lab}} + v_{LT} f_{LT} \cos \phi_p^{\mathrm{lab}}\Big]. \quad (1)$$

Here Ω_e^{lab} and Ω_p^{lab} are the solid angles of the electron and the proton, k^{lab} and k'^{lab} are the magnitude of incoming and outgoing electron 3-momenta, Q_{lab}^2 is the 4-momentum-squared of the virtual photon, and α is the fine structure constant. ϕ_p^{lab} is the angle between the

scattering plane containing the electrons and the plane spanned by outgoing nucleons. $v_L, v_T, \ldots$ are electron kinematic factors, and $f_L, f_T, \ldots$ are the deuteron structure functions. These structure functions contain all the dynamic information about the process. The four structure functions are independent and can be separated by combining cross-section measurements carried out with appropriate kinematic settings [39]. Structure functions are thus cross sections up to kinematic factors and are independent of the SRG scale λ. In this work we focus on the longitudinal structure function f_L, following the approach of Ref. [34].

B. Calculating f_L

As in Ref. [34], we carry out the calculations in the center-of-mass frame of the outgoing proton-neutron pair. In this frame the photon four-momentum is $(\omega, \mathbf{q})$, which can be obtained from the initial electron energy and θ_e, the electron scattering angle. We denote the momentum of the outgoing proton by $\mathbf{p}'$ and take $\mathbf{q}$ to be along z-axis. The angles of $\mathbf{p}'$ are denoted by $\Omega_{\mathbf{p}'} = (\theta', \varphi')$.

The longitudinal structure function can be written as

$$f_L = \sum_{\substack{S_f, m_{s_f} \\ m_{J_d}}} \mathcal{T}_{S_f, m_{s_f}, \mu=0, m_{J_d}}(\theta', \varphi')\,\mathcal{T}^*_{S_f, m_{s_f}, \mu=0, m_{J_d}}(\theta', \varphi'),$$

$$(2)$$

where S_f and m_{s_f} are the spin quantum numbers of the final neutron-proton state, μ is the Lorentz index of the current, and m_{J_d} is the angular momentum of the initial deuteron state. The amplitude $\mathcal{T}$ is given by [40]

$$\mathcal{T}_{S, m_{s_f}, \mu, m_{J_d}} = -\pi\sqrt{2\alpha|\mathbf{p}'|E_p E_d/M_d}\,\langle\psi_f\,|\,J_\mu(\mathbf{q})\,|\psi_i\rangle,$$
$$(3)$$

where $\langle\psi_f|$ is the final-state wavefunction of the outgoing neutron-proton pair, $|\psi_i\rangle$ is the initial deuteron state, and $J_\mu(\mathbf{q})$ is the current operator that describes the momentum transferred by the photon. The variables in Eq. (3) are:

- fine-structure constant α;

- outgoing proton (neutron) 3-momentum $\mathbf{p}'\,(-\mathbf{p}')$;

- proton energy $E_p = \sqrt{M^2 + \mathbf{p}'^2}$, where M is the average of proton and neutron mass

- deuteron energy $E_d = \sqrt{M_d^2 + \mathbf{q}^2}$, where M_d is the mass of the deuteron.

As mentioned before, all of these quantities are in the center-of-mass frame of the outgoing nucleons.

For f_L, only the $\mu = 0$ component of $\mathcal{T}$ and therefore only the zeroth component of the current contributes.

The one-body current matrix element is given by

$$
\langle \mathbf{k}_1 \, T_1 | \, J_0(\mathbf{q}) \, | \, \mathbf{k}_2 \, T = 0 \rangle
$$
$$
= \frac{1}{2} \left(G_E^p + (-1)^{T_1} G_E^n \right) \delta(\mathbf{k}_1 - \mathbf{k}_2 - \mathbf{q}/2)
$$
$$
+ \frac{1}{2} \left((-1)^{T_1} G_E^p + G_E^n \right) \delta(\mathbf{k}_1 - \mathbf{k}_2 + \mathbf{q}/2) \,, \quad (4)
$$

where G_E^p and G_E^n are the electric form factors of the proton and the neutron, and the deuteron state has isospin $T = 0$.

The final-state wave function of the outgoing proton-neutron pair can be written as

$$
|\psi_f\rangle = |\phi\rangle + G_0(E') \, t(E') \, |\phi\rangle \,, \quad (5)
$$

where $|\phi\rangle$ denotes a relative plane wave, G_0 and t are the Green's function and the t-matrix respectively, and

$E' = \mathbf{p}'^2/M$ is the energy of the outgoing nucleons. The second term in Eq. (5) describes the interaction between the outgoing nucleons.

In the impulse approximation (IA) as defined here, the interaction between the outgoing nucleons is ignored and $|\psi_f\rangle_{\text{IA}} \equiv |\phi\rangle$. The plane wave $|\phi\rangle$ will have both isospin 0 and 1 components. The current J_0, G_0, and the t-matrix are diagonal in spin space. The deuteron has spin $S = 1$ and therefore the final state will also have $S = 1$. Hence, we have

$$
|\phi\rangle \equiv |\mathbf{p}' \, S = 1 \, m_{s_f} \psi_T\rangle
$$
$$
= \frac{1}{2} \sum_{T=0,1} \Big(|\mathbf{p}' \, S = 1 \, m_{s_f}\rangle \qquad\qquad (6)
$$
$$
+ (-1)^T |{-}\mathbf{p}' \, S = 1 \, m_{s_f}\rangle \Big) |T\rangle \,.
$$

Using Eqs. (4) and (6), the overlap matrix element in IA becomes

$$
\langle \psi_f | \, J_0 \, | \psi_i \rangle_{\text{IA}} = \sqrt{\frac{2}{\pi}} \sum_{L_d = 0,2} \langle L_d \, m_{J_d} - m_{s_f} \, S = 1 \, m_{s_f} | J = 1 \, m_{J_d} \rangle
$$
$$
\times \left[G_E^p \, \psi_{L_d}(|\mathbf{p}' - \mathbf{q}/2|) \, Y_{L_d, m_{J_d} - m_{s_f}}(\Omega_{\mathbf{p}'-\mathbf{q}/2}) + G_E^n \, \psi_{L_d}(|\mathbf{p}' + \mathbf{q}/2|) \, Y_{L_d, m_{J_d} - m_{s_f}}(\Omega_{\mathbf{p}'+\mathbf{q}/2}) \right], \quad (7)
$$

where $\Omega_{\mathbf{p}' \pm \mathbf{q}/2}$ is the solid angle between the unit vector $\hat{z}$ and $\mathbf{p}' \pm \mathbf{q}/2$. ψ_{L_d} is the deuteron wave function in momentum space defined as

$$
\langle k_1 \, J_1 \, m_{J_1} \, L_1 \, S_1 \, T_1 | \psi_i \rangle = \psi_{L_1}(k_1)
$$
$$
\times \delta_{J_1,1} \delta_{m_{J_1}, m_{J_d}} \delta_{L_1, L_d} \delta_{S_1, 1} \delta_{T_1, 0} \,. \quad (8)
$$

The S-wave ($L = 0$) and D-wave ($L = 2$) components of the deuteron wave function satisfy the normalization condition

$$
\frac{2}{\pi} \int dp \, p^2 \left(\psi_0^2(p) + \psi_2^2(p) \right) = 1 \,. \quad (9)
$$

In deriving Eq. (7) we have used the property of the spherical harmonics that

$$
Y_{lm}(\pi - \theta, \phi + \pi) = (-1)^l \, Y_{lm}(\theta, \phi) \,. \quad (10)
$$

In our work we follow the conventions of Ref. [41]. Since θ' and φ' are the angles of $\mathbf{p}'$, $\Omega_{\mathbf{p}'-\mathbf{q}/2} \equiv \left(\alpha'(p', \theta'), \varphi' \right)$ and $\Omega_{\mathbf{p}'+\mathbf{q}/2} \equiv \left(\alpha''(p', \theta'), \varphi' \right)$, where

$$
\alpha'(p', \theta') = \cos^{-1} \left(\frac{p' \cos\theta' - q/2}{\sqrt{p'^2 - p'q \cos\theta' + q^2/4}} \right) \quad (11)
$$

and

$$
\alpha''(p', \theta') = \cos^{-1} \left(\frac{p' \cos\theta' + q/2}{\sqrt{p'^2 + p'q \cos\theta' + q^2/4}} \right) \,. \quad (12)
$$

The overlap matrix element including the final-state interactions (FSI) is given by

$$
\langle \psi_f | \, J_0 \, | \psi_i \rangle = \underbrace{\langle \phi | \, J_0 \, | \psi_i \rangle}_{\text{IA}} + \underbrace{\langle \phi | t^\dagger \, G_0^\dagger \, J_0 \, | \psi_i \rangle}_{\text{FSI}} \,. \quad (13)
$$

The first term on the right side of Eq. (13) has already been evaluated in Eq. (7). Therefore, the term we still need to evaluate is $\langle \phi | t^\dagger \, G_0^\dagger \, J_0 \, | \psi_i \rangle$. The t-matrix is most conveniently calculated in a partial-wave basis. Hence, the FSI term is evaluated by inserting complete sets of states in the form

$$
1 = \frac{2}{\pi} \sum_{\substack{L,S \\ J,m_J}} \sum_{T=0,1} \int dp \, p^2 \, |p \, J \, m_J \, L \, S \, T\rangle \, \langle p \, J \, m_J \, L \, S \, T| \,.
$$
$$
(14)
$$

The outgoing plane-wave state in the partial-wave basis is given by

$$
\langle \phi | \, k_1 \, J_1 \, m_{J_1} \, L_1 \, S = 1 \, T_1 \rangle = \frac{1}{2} \sqrt{\frac{2}{\pi}} \frac{\pi}{2} \frac{\delta(p' - k_1)}{k_1^2}
$$
$$
\times \langle L_1 \, m_{J_1} - m_{s_f} \, S = 1 \, m_{s_f} | J_1 \, m_{J_1} \rangle
$$
$$
\times \left(1 + (-1)^{T_1} (-1)^{L_1} \right) Y_{L_1, m_{J_1} - m_{s_f}}(\theta', \varphi') \,. \quad (15)
$$

The Green's function is diagonal in J, m_J, L, S, and T, so we have

$$
\langle k_1 | \, G_0^\dagger \, | k_2 \rangle = \frac{\pi}{2} \frac{\delta(k_1 - k_2)}{k_1^2} \frac{M}{p'^2 - k_1^2 - i\epsilon} \,. \quad (16)
$$

We also need to express the current in Eq. (4) in the partial-wave basis. To begin with, let us just work with the first term in Eq. (4), which we denote by J_0^-. In the partial-wave basis, it is written as

$$\langle k_1\, J_1\, m_{J_d}\, L_1\, S = 1\, T_1 | J_0^- | k_2\, J = 1\, m_{J_d}\, L_2\, S = 1\, T = 0 \rangle = \frac{\pi^2}{2} \left(G_E^p + (-1)^{T_1}\, G_E^n \right)$$

$$\times \sum_{\widetilde{m}_s = -1}^{1} \int \mathrm{dcos}\,\theta\, \langle J_1\, m_{J_d} | L_1\, m_{J_d} - \widetilde{m}_s\, S = 1\, \widetilde{m}_s \rangle\, P_{L_1}^{m_{J_d} - \widetilde{m}_s}(\cos\theta)\, P_{L_2}^{m_{J_d} - \widetilde{m}_s}\!\left(\cos\alpha'(k_1, \theta) \right)$$

$$\times \frac{\delta\!\left(k_2 - \sqrt{k_1^2 - k_1 q \cos\theta + q^2/4} \right)}{k_2^2}\, \langle L_2\, m_{J_d} - \widetilde{m}_s\, S = 1\, \widetilde{m}_s | J = 1\, m_{J_d} \rangle . \quad (17)$$

Here m_{J_d} is the deuteron quantum number, which is preserved throughout. We have used the deuteron quantum numbers in the ket in anticipation that we will always evaluate the matrix element of J_0 with the deuteron wave function on the right. α' is as defined in Eq. (11). In deriving Eq. (17) we have also made use of the relation [42]

$$\int Y_{lm}^*(\theta, \varphi)\, Y_{l'm'}(\theta', \varphi)\, \mathrm{dcos}\,\theta\, \mathrm{d}\varphi = 2\pi \delta_{mm'} \int \mathrm{dcos}\,\theta\, P_l^m(\cos\theta)\, P_{l'}^m(\cos\theta') . \quad (18)$$

Equations (15), (16), and (17) can be combined to obtain

$$\langle \phi | t^\dagger\, G_0^\dagger\, J_0^- | \psi_i \rangle = \sqrt{\frac{2}{\pi}}\, \frac{M}{\hbar c} \sum_{T_1 = 0, 1} \left(G_E^p + (-1)^{T_1}\, G_E^n \right) \sum_{L_1 = 0}^{L_{\max}} \left(1 + (-1)^{T_1} (-1)^{L_1} \right) Y_{L_1, m_{J_d} - m_{s_f}}(\theta', \varphi')$$

$$\times \sum_{J_1 = |L_1 - 1|}^{L+1} \langle L_1\, m_{J_d} - m_{s_f}\, S = 1\, m_{s_f} | J_1\, m_{J_d} \rangle \sum_{L_2 = 0}^{L_{\max}} \int \mathrm{d}k_2\, k_2^2\, t^*(k_2, p', L_2, L_1, J_1, S = 1, T_1)$$

$$\times \sum_{\widetilde{m}_s = -1}^{1} \langle J_1\, m_{J_d} | L_2\, m_{J_d} - \widetilde{m}_s\, S = 1\, \widetilde{m}_s \rangle \sum_{L_d = 0, 2} \langle L_d\, m_{J_d} - \widetilde{m}_s\, S = 1\, \widetilde{m}_s | J = 1\, m_{J_d} \rangle$$

$$\times \int \mathrm{dcos}\,\theta\, \frac{1}{p'^2 - k_2^2 - i\epsilon}\, P_{L_2}^{m_{J_d} - \widetilde{m}_s}(\cos\theta)\, P_{L_d}^{m_{J_d} - \widetilde{m}_s}\!\left(\cos\alpha'(k_2, \theta) \right) \psi_{L_d}\!\left(\sqrt{k_2^2 - k_2 q \cos\theta + q^2/4} \right) . \quad (19)$$

We denote the second term in the one-body current Eq. (4) by J_0^+. The expression for $\langle \phi | t^\dagger\, G_0^\dagger\, J_0^+ | \psi_i \rangle$ is analogous to Eq. (19), the only differences being that the form-factor coefficient is $(-1)^{T_1} G_E^p + G_E^n$ and the input arguments for the second associated Legendre polynomial and the deuteron wave function are different. The two factors respectively become $P_{L_d}^{m_{J_d} - \widetilde{m}_s}\!\left(\cos\alpha''(k_2, \theta) \right)$ and $\psi_{L_d}\!\left(\sqrt{k_2^2 + k_2 q \cos\theta + q^2/4} \right)$, where α'' is defined in Eq. (12). It can be shown that $\langle \phi | t^\dagger\, G_0^\dagger\, J_0^+ | \psi_i \rangle = \langle \phi | t^\dagger\, G_0^\dagger\, J_0^- | \psi_i \rangle$. Thus,

$$\langle \phi | t^\dagger\, G_0^\dagger\, J_0 | \psi_i \rangle = 2 \langle \phi | t^\dagger\, G_0^\dagger\, J_0^- | \psi_i \rangle . \quad (20)$$

Using this we can evaluate the overlap matrix element in Eq. (13). As outlined in Eqs. (2) and (3), this matrix element is related to the longitudinal structure function f_L. Recall that the deuteron spin is conserved throughout and therefore $S_f = 1$ in Eq. (2).

In Sec. III C we present results for f_L both in the IA and including the FSI. These results match those of Ref. [34, 40], verifying the accuracy of the calculations presented above.

C. Evolution setup

As outlined in the introduction, we want to investigate the effect of unitary transformations on calculations of f_L. Let us start by looking at the IA matrix element:

$$\langle \phi | J_0 | \psi_i \rangle = \langle \phi | U^\dagger\, U\, J_0\, U^\dagger\, U | \psi_i \rangle$$
$$= \underbrace{\langle \phi | \widetilde{U}^\dagger\, J_0^\lambda | \psi_i^\lambda \rangle}_{A} + \underbrace{\langle \phi | J_0^\lambda | \psi_i^\lambda \rangle}_{B} , \quad (21)$$

where we decompose the unitary matrix U into the identity and a residual $\widetilde{U}$,

$$U = I + \widetilde{U} . \quad (22)$$

The matrix $\widetilde{U}$ is smooth and therefore amenable to interpolation. The U matrix is calculated following the

approach in [4]. The terms in Eq. (21) can be further split into

$$\langle\phi|\,J_0^\lambda|\psi_i^\lambda\rangle = \underbrace{\langle\phi|\widetilde{U}\,J_0\,\widetilde{U}^\dagger|\psi_i^\lambda\rangle}_{B_1} + \underbrace{\langle\phi|\widetilde{U}\,J_0\,|\psi_i^\lambda\rangle}_{B_2}$$
$$+ \underbrace{\langle\phi|\,J_0\,\widetilde{U}^\dagger|\psi_i^\lambda\rangle}_{B_3} + \underbrace{\langle\phi|\,J_0\,|\psi_i^\lambda\rangle}_{B_4} \quad (23)$$

and

$$\langle\phi|\widetilde{U}^\dagger J_0^\lambda|\psi_i^\lambda\rangle$$
$$= \underbrace{\langle\phi|\widetilde{U}^\dagger\,\widetilde{U}\,J_0\,\widetilde{U}^\dagger|\psi_i^\lambda\rangle}_{A_1} + \underbrace{\langle\phi|\widetilde{U}^\dagger\,\widetilde{U}\,J_0|\psi_i^\lambda\rangle}_{A_2}$$
$$+ \underbrace{\langle\phi|\widetilde{U}^\dagger J_0\,\widetilde{U}^\dagger|\psi_i^\lambda\rangle}_{A_3} + \underbrace{\langle\phi|\widetilde{U}^\dagger J_0|\psi_i^\lambda\rangle}_{A_4}. \quad (24)$$

The B_4 term is the same as in Eq. (7), but with the deuteron wave function replaced by the evolved version $\psi_{L_d}^\lambda$. Inserting complete sets of partial-wave basis states as in Eq. (14) and using Eqs. (15) and (17), we can obtain the expressions for B_1, B_2, B_3 and $A_1,\ldots,A_4$. These expressions are given in Appendix A.

Using the expressions for $A_1,\ldots,A_4$ and $B_1,\ldots,B_4$, we can obtain results for f_L in the IA with one or more components of the overlap matrix element $\langle\phi|J_0|\psi\rangle$ evolved. When calculated in IA, f_L with all components evolved matches its unevolved counterpart, as shown later in Sec. III C. The robust agreement between the evolved and unevolved answers indicates that the expressions derived for $A_1,\ldots,B_4$ are correct and that there is no error in generating the U-matrices. In Sec. II D we provide some details about the numerical implementation of the equations presented here.

Let us now take into account the FSI and study the effects of evolution. The overlap matrix element should again be unchanged under evolution,

$$\langle\psi_f|J_0|\psi_i\rangle = \langle\psi_f^\lambda|J_0^\lambda|\psi_i^\lambda\rangle, \quad (25)$$

where ψ_f is given by Eq. (5). Furthermore,

$$|\psi_f^\lambda\rangle = |\phi\rangle + G_0\,t_\lambda|\phi\rangle, \quad (26)$$

where t_λ is the evolved t-matrix, *i.e.*, the t-matrix obtained by solving the Lippmann–Schwinger equation using the evolved potential, as discussed in Appendix B. Thus

$$\langle\psi_f^\lambda|J_0^\lambda|\psi_i^\lambda\rangle = \underbrace{\langle\phi|J_0^\lambda|\psi_i^\lambda\rangle}_{B} + \underbrace{\langle\phi|t_\lambda^\dagger\,G_0^\dagger\,J_0^\lambda|\psi_i^\lambda\rangle}_{F}. \quad (27)$$

The term B is the same that we already encountered in

Eq. (21). The term F can also be split up into four terms:

$$\langle\phi|t_\lambda^\dagger\,G_0^\dagger\,J_0^\lambda|\psi_i^\lambda\rangle$$
$$= \underbrace{\langle\phi|t_\lambda^\dagger\,G_0^\dagger\,\widetilde{U}\,J_0\,\widetilde{U}^\dagger|\psi_i^\lambda\rangle}_{F_1} + \underbrace{\langle\phi|t_\lambda^\dagger\,G_0^\dagger\,\widetilde{U}\,J_0|\psi_i^\lambda\rangle}_{F_2}$$
$$+ \underbrace{\langle\phi|t_\lambda^\dagger\,G_0^\dagger\,J_0\,\widetilde{U}^\dagger|\psi_i^\lambda\rangle}_{F_3} + \underbrace{\langle\phi|t_\lambda^\dagger\,G_0^\dagger\,J_0|\psi_i^\lambda\rangle}_{F_4}. \quad (28)$$

The expression for F_4 can easily be obtained from Eqs. (19) and (20) by replacing the deuteron wave function and the t-matrix by their evolved counterparts. As before, we insert complete sets of partial-wave basis states using Eq. (14) and evaluate F_3, F_2, and F_1; see Eqs. (A6), (A7), and (A8). Figures in Sec. III C compare f_L calculated from the matrix element with all components evolved to the unevolved f_L. We find an excellent agreement, validating the expressions for $F_1,\ldots,F_4$.

D. Numerical implementation

There are various practical issues in the calculation of evolved matrix elements that are worth detailing. We use C++11 for our numerical implementation of the expressions discussed in the previous section. Matrix elements with a significant number of components evolved are computationally quite expensive due to a large number of nested sums and integrals (see in particular Appendix A).

The deuteron wave function and NN t-matrix are obtained by discretizing the Schrödinger and Lippmann–Schwinger equations, respectively; these equations are also used to interpolate the t-matrix and wave function to points not on the discretized mesh. For example, if we write the momentum-space Schrödinger equation—neglecting channel coupling here for simplicity—as

$$\psi(p) = \int \mathrm{d}q\,q^2\,G_0(-E_B,q)V(p,q)\,\psi(q)$$
$$\to \sum_i w_i\,q_i^2\,G_0(-E_B,q_i)V(p,q_i)\,\psi(q_i), \quad (29)$$

it can be solved numerically as a simple matrix equation by setting $p \in \{q_i\}$. For any $p = p_0$ not on this mesh, the sum in Eq. (29) can then be evaluated to get $\psi(p_0)$. This technique is based on what has been introduced in connection with contour-deformation methods in breakup scattering calculations [43, 44].

To interpolate the potential, which is stored on a momentum-space grid, we use the two-dimensional cubic spline algorithm from ALGLIB [45]. In order to avoid unnecessary recalculation of expensive quantities—in particular of the off-shell t-matrix—while still maintaining an implementation very close to the expressions given in this paper, we make use of transparent caching tech-

niques.[2] For most integrations, in particular those involving a principal value, we use straightforward nested Gaussian quadrature rules; only in a few cases did we find it more efficient to use adaptive routines for multi-dimensional integrals.

With these optimizations, the calculations can in principle still be run on a typical laptop computer. In practice, we find it more convenient to use a small cluster, with parallelization implemented using the TBB library [46]. On a node with 48 cores, generating data for a meaningful plot (like those shown in Sec. III) can then be done in less than an hour. For higher resolution and accuracy, we used longer runs with a larger number of data and integration mesh points.

III. EFFECTS OF UNITARY EVOLUTION

A. First order analytical calculation

Recall that from Eqs. (2) and (3) we have

$$f_L \propto \sum_{m_{s_f}, m_{J_d}} |\langle \psi_f | J_0 | \psi_i \rangle|^2 \,. \tag{30}$$

When all three components—the final state, the current, and the initial state—are evolved consistently, then f_L is unchanged. However, if we miss evolving a component, then we obtain a different result. It is instructive to illustrate this through a first-order analytical calculation.[3]

Let us look at the effects due to the evolution of individual components for a general matrix element $\langle \psi_f | \widehat{O} | \psi_i \rangle$. The evolved initial state is given by

$$|\psi_i^\lambda\rangle \equiv U |\psi_i\rangle = |\psi_i\rangle + \widetilde{U} |\psi_i\rangle \,, \tag{31}$$

where $\widetilde{U}$ is the smooth part of the U-matrix defined in Eq. (22). Similarly, we can write down the expressions for the evolved final state and the evolved operator as

$$\langle \psi_f^\lambda | \equiv \langle \psi_f | U^\dagger = \langle \psi_f | - \langle \psi_f | \widetilde{U} \tag{32}$$

and

$$\widehat{O}^\lambda \equiv U \widehat{O} U^\dagger = \widehat{O} + \widetilde{U} \widehat{O} - \widehat{O} \widetilde{U} + \mathcal{O}(\widetilde{U}^2) \,. \tag{33}$$

We assume here that $\widetilde{U}$ is small compared to I (which can always be ensured by choosing the SRG λ large enough)

and therefore keep terms only up to linear order in $\widetilde{U}$. Using Eqs. (31), (32), and (33), we get an expression for the evolved matrix element in terms of the unevolved one and changes to individual components due to evolution:

$$\langle \psi_f^\lambda | \widehat{O}^\lambda | \psi_i^\lambda \rangle = \langle \psi_f | \widehat{O} | \psi_i \rangle - \underbrace{\langle \psi_f | \widetilde{U} \widehat{O} | \psi_i \rangle}_{\delta \langle \psi_f |}$$

$$+ \underbrace{\langle \psi_f | \widetilde{U} \widehat{O} | \psi_i \rangle - \langle \psi_f | \widehat{O} \widetilde{U} | \psi_i \rangle}_{\delta \widehat{O}} + \underbrace{\langle \psi_f | \widehat{O} \widetilde{U} | \psi_i \rangle}_{\delta | \psi_i \rangle} \quad (34)$$

$$\implies \langle \psi_f^\lambda | \widehat{O}^\lambda | \psi_i^\lambda \rangle = \langle \psi_f | \widehat{O} | \psi_i \rangle + \mathcal{O}(\widetilde{U}^2) \,. \tag{35}$$

We see that the change due to evolution in the operator is equal and opposite to the sum of changes due to the evolution of the initial and final states. We also find that changes in each of the components are of the same order, and that they mix; this feature persists to higher order. Therefore, if one misses evolving an individual component, one will not reproduce the unevolved answer.

B. Overview of numerical results

For our analysis, we studied the effect of evolution of individual components on f_L for selected kinematics in the ranges $E' = 10$–100 MeV and $\mathbf{q}^2 = 0.25$–25 fm^{-2}, where E' is the energy of outgoing nucleons and $\mathbf{q}^2$ is the three-momentum transferred by the virtual photon; both are taken in the center-of-mass frame of the outgoing nucleons. This range was chosen to cover a variety of kinematics and motivated by the set covered in Ref. [34]. We use the Argonne v_{18} potential (AV18) [48] for our calculations. It is one of the widely used potentials for nuclear few-body reaction calculations, particularly those involving large momentum transfers [19, 49].

How strong the evolution of individual components (or a subset thereof) affects the result for f_L depends on the kinematics. One kinematic configuration of particular interest is the so-called quasi-free ridge. As discussed in Sec. II A, the four-momentum transferred by the virtual photon in the center-of-mass frame is $(\omega, \mathbf{q})$. The criterion for a configuration to lie on the quasi-free ridge is $\omega = 0$. Physically, this means that the nucleons in the deuteron are on their mass shell. As shown in Ref. [34], at the quasi-free ridge the energy of the outgoing nucleons (E') and the photon momentum transfer are related by

$$E' = \sqrt{M_d^2 + \mathbf{q}^2} - 2M \,, \tag{36}$$

which reduces to

$$E' \text{ (in MeV)} \approx 10 \, \mathbf{q}^2 \text{ (in fm}^{-2}) \,. \tag{37}$$

The quasi-free condition in the center-of-mass frame is the same as the quasi-elastic condition in the lab frame.

---

[2] This means that the expensive calculation is only carried out once, the first time the corresponding function is called for a given set of arguments, while subsequent calls with the same arguments return the result directly, using a fast lookup. All this is done without the *calling* code being aware of the caching details.

[3] An analogous calculation based on field redefinitions appears in Ref. [47].

There, the quasi-elastic ridge is defined by $W^2 = m_p^2 \Rightarrow Q^2 = 2\omega_{\mathrm{lab}} m_p$, where W is the invariant mass. On the quasi-elastic ridge, the so-called missing momentum[4] vanishes, $p_{\mathrm{miss}} = 0$.

In Fig. 2 we plot f_L along the quasi-free ridge both in the impulse approximation (IA) and with the final-state interactions (FSI) included as a function of energy of the outgoing nucleons for a fixed angle, $\theta' = 15^{\circ}$ of the outgoing proton. E' and $\mathbf{q}^2$ in Fig. 2 are related by Eq. (36). Comparing the solid curve labeled $\langle\psi_f|J_0|\psi_i\rangle$ in the legend to the dashed curve (labeled $\langle\phi|J_0|\psi_i\rangle$) we find that FSI effects are minimal for configurations on the quasi-free ridge especially at large energies.
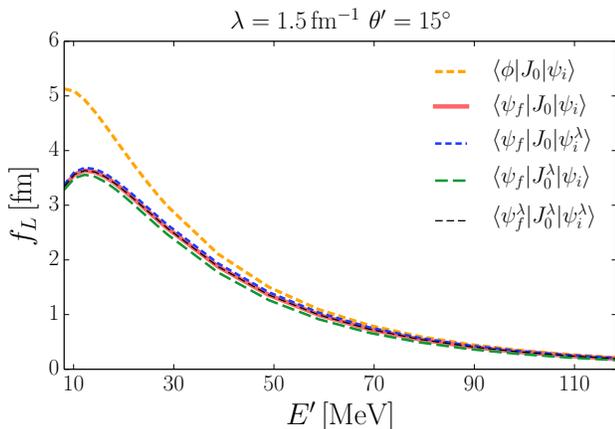
Figure 2. (color online) f_L calculated at various points on the quasi-free ridge for $\theta' = 15^{\circ}$ for the AV18 potential. Legends indicate which component of the matrix element in Eq. (30) used to calculate f_L is evolved. There are no appreciable effects due to the evolution all along the quasi-free ridge. The effect due to evolution of the final state is small as well and is not shown here to avoid clutter. f_L calculated in the impulse approximation is also shown for comparison.

In an intuitive picture, this is because after the initial photon is absorbed, both the nucleons in the deuteron are on their mass shell at the quasi-free ridge, and therefore no FSI are needed to make the final-state particles real. As we move away from the ridge, FSI become more important, as additional energy-momentum transfer is required to put the neutron and the proton on shell in the final state. The difference between full f_L and f_L in IA at small energies is also seen to hold for few-body nuclei [50].

Figure 2 also shows f_L calculated from evolving only one of the components of the matrix element in Eq. (30). We note that the effects of SRG evolution of the individual components are minimal at the quasi-free ridge

---

[4] The missing momentum is defined as the difference of the measured proton momentum and the momentum transfer, $\mathbf{p}_{\mathrm{miss}} \equiv \mathbf{p}_{\mathrm{lab}}^{\mathrm{proton}} - \mathbf{q}_{\mathrm{lab}}$.

as well. The kinematics at the quasi-free ridge are such that only the long-range (low-momentum) part of the deuteron wave function is probed, the FSI remains small under evolution, and then unitarity implies minimal evolution of the current. As one moves away from the quasi-free ridge, the effects of evolution of individual components become prominent. Note that $\langle\psi_f|J_0|\psi_i\rangle = \langle\psi_f^{\lambda}|J_0^{\lambda}|\psi_i^{\lambda}\rangle$ and therefore the unevolved vs. all-evolved f_L overlap in Fig. 2.
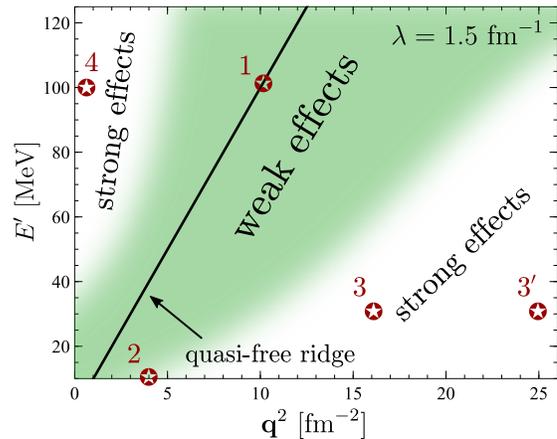

Figure 3. (color online) 'Phase space' of kinematics for $\lambda = 1.5\,\mathrm{fm}^{-1}$. The effects of evolution get progressively prominent as one moves further away from the quasi-free ridge. The kinematics of the labeled points are considered in Sec. III C.

Figure 3 shows the 'phase space' of kinematics for SRG $\lambda = 1.5$ fm^{-1}. The quasi-free ridge is along the solid line in Fig. 3. In the shaded region the effects due to evolution of individual components are weak (only a few percent relative difference). As one moves away from the quasi-free ridge, these differences get progressively more prominent. The terms 'small' and 'weak' in Fig. 3 are used in a qualitative sense. In the shaded region denoted by 'weak effects', the effects of evolution are not easily discernible on a typical f_L versus θ' plot, as seen in Fig. 4, whereas in the region labeled by 'strong effects', the differences due to evolution are evident on a plot (e.g., see Fig. 6). The size of the shaded region in Fig. 3 depends on the SRG λ. It is large for high λ's and gets smaller as the λ is decreased (note that smaller SRG λ means greater evolution). In the next subsection we look in detail at a few representative kinematics, indicated by points in Fig. 3.

C. Illustrative examples

1. At the quasi-free ridge

As a representative of quasi-free kinematics, we choose $E' = 100$ MeV and $\mathbf{q}^2 = 10$ fm^{-2} and plot f_L as a function of angle in Fig. 4. The effect of including FSI is small for this configuration for all angles. Also, the

effects due to evolution of the individual components are too small to be discernible. All this is consistent with the discussion in the previous section.
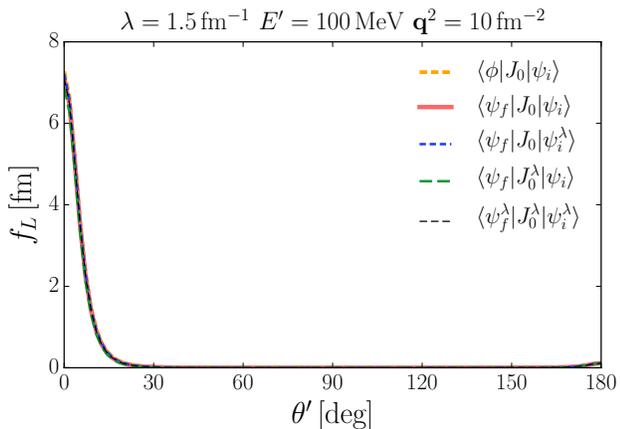

Figure 4. (color online) f_L calculated for $E' = 100$ MeV and $\mathbf{q}^2 = 10$ fm^{-2} (point "1" in Fig. 3) for the AV18 potential. Legends indicate which component of the matrix element in Eq. (30) used to calculate f_L is evolved. θ' is the angle of the outgoing proton in the center-of-mass frame. There are no discernible effects due to the evolution for all angles. The effect due to evolution of the final state is small as well and is not shown here to avoid clutter. f_L calculated in the IA, $\langle \phi | J_0 | \psi_i \rangle$, is also shown for comparison.

2. Near the quasi-free ridge

Next we look at the kinematics $E' = 10$ MeV and $\mathbf{q}^2 = 4$ fm^{-2}, which is near the quasi-free ridge. This is the point "2" in Fig. 3. As seen in Fig. 5, the different curves for f_L obtained from evolving different components start to diverge. Figure 5 also shows f_L calculated in IA. Comparing this to the full f_L including FSI, we see that the effects due to evolution are small compared to the FSI contributions. This smallness prevents us from making any systematic observations about the effects due to evolution at this kinematics. We thus move on to kinematics which show more prominent effects.

3. Below the quasi-free ridge

We next look in the region where E' (in MeV) $\ll 10\,\mathbf{q}^2$ (in fm^{-2}), i.e., below the quasi-free ridge in Fig. 3. We look at two momentum transfers $\mathbf{q}^2 = 16$ fm^{-2} and $\mathbf{q}^2 = 25$ fm^{-2} for $E' = 30$ MeV, which are points "3" and "3'" in Fig. 3. Figures 6 and 7 indicate the effects on f_L from evolving individual components of the matrix elements. It is noteworthy that in both cases evolution of the current gives a prominent enhancement, whereas evolution of the initial and final state gives a suppression. When all the components are evolved consistently, these
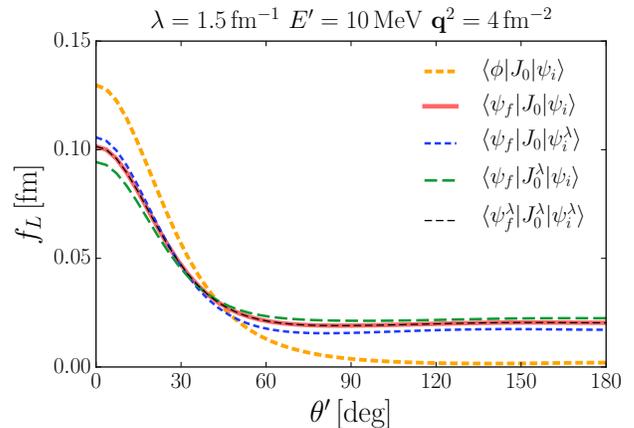

Figure 5. (color online) f_L calculated for $E' = 10$ MeV and $\mathbf{q}^2 = 4$ fm^{-2} (point "2" in Fig. 3) for the AV18 potential. Legends indicate which component of the matrix element in Eq. (30) used to calculate f_L is evolved. f_L calculated in the IA, $\langle \phi | J_0 | \psi_i \rangle$, is also shown for comparison. The effects due to evolution of individual components on f_L are discernible, but still small (compared to the FSI contribution). The effect due to evolution of the final state is small as well and is not shown here to avoid clutter.

changes combine and we recover the unevolved answer for f_L. This verifies the accurate implementation of the equations derived in Sec. II C.
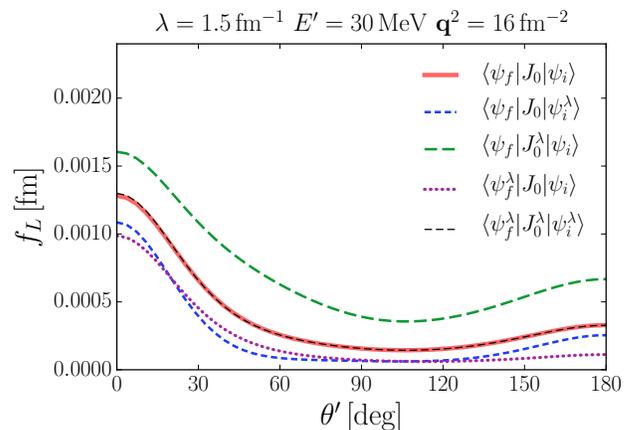

Figure 6. (color online) f_L calculated for $E' = 30$ MeV and $\mathbf{q}^2 = 16$ fm^{-2} (point "3" in Fig. 3) for the AV18 potential. Legends indicate which component of the matrix element in Eq. (30) used to calculate f_L is evolved. Prominent enhancement with evolution of the current only and suppression with evolution of the initial state and the final state only, respectively.

It is possible to qualitatively explain the behavior seen in Figs. 6 and 7. As noted in Eq. (13), the overlap matrix element is given by the sum of the IA part and the FSI part. Below the quasi-free ridge these two terms add constructively. In this region, f_L calculated in impulse
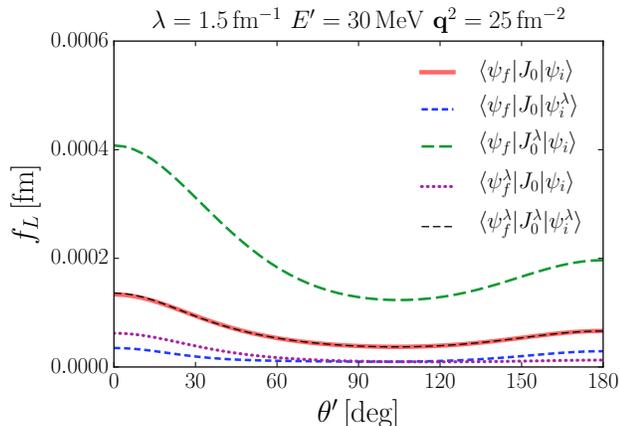
Figure 7. (color online) f_L calculated for $E' = 30$ MeV and $\mathbf{q}^2 = 25$ fm^{-2} (point "3" in Fig. 3) for the AV18 potential. Legends indicate which component of the matrix element in Eq. (30) used to calculate f_L is evolved. Prominent enhancement with evolution of the current only and suppression with evolution of the initial state and the final state only, respectively.
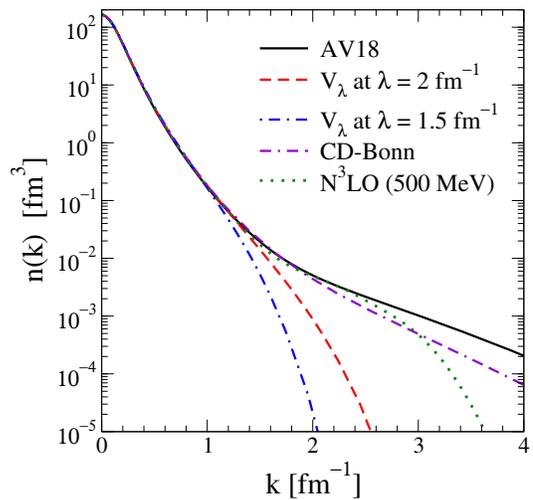

Figure 8. (color online) Momentum distribution for the deuteron for the AV18 [48], CD-Bonn [51], and the Entem-Machleidt N^{3}LO chiral EFT [52] potentials, and for the AV18 potential evolved to two SRG λ's.

approximation is smaller than f_L calculated by including the final-state interactions.

a. Evolving the initial state Let us first consider the effect of evolving the initial state only. We have

$$\langle\psi_f|J_0|\psi_i^\lambda\rangle = \langle\phi|J_0|\psi_i^\lambda\rangle + \langle\phi|t^\dagger\,G_0^\dagger\,J_0|\psi_i^\lambda\rangle. \qquad (38)$$

As seen in Eq. (7), in the term $\langle\phi|J_0|\psi_i^\lambda\rangle$ the deuteron wave function is probed between $|p' - q/2|$ and $p' + q/2$. These numbers are $(1.2, 2.9)$ fm^{-1} and $(1.7, 3.4)$ fm^{-1} for $E' = 30$ MeV, $\mathbf{q}^2 = 16$ fm^{-2} and $E' = 30$ MeV, $\mathbf{q}^2 = 25$ fm^{-2}, respectively. The evolved deuteron wave function is significantly suppressed at these high momenta. This behavior is reflected in the deuteron momentum distribution plotted in Fig. 8. The deuteron momentum distribution $n(k)$ is proportional to the sum of the squares of S- and D- state deuteron wave functions. Thus, the first (IA) term in Eq. (38) is much smaller than its unevolved counterpart in Eq. (13), for all angles. We note that even though we only use the AV18 potential to study changes due to evolution, these changes will be significant for other potentials as well.

Evaluation of the second (FSI) term in Eq. (38) involves an integral over all momenta, as indicated in Eq. (19). We find that $|\langle\phi|t^\dagger\,G_0^\dagger\,J_0|\psi_i^\lambda\rangle| < |\langle\phi|t^\dagger\,G_0^\dagger\,J_0|\psi_i\rangle|$. As mentioned before, because the terms $\langle\phi|J_0|\psi_i\rangle$ and $\langle\phi|t^\dagger\,G_0^\dagger\,J_0|\psi_i\rangle$ add constructively below the quasi-free ridge and because the magnitude of both these terms decreases upon evolving the wave function, we have

$$|\langle\psi_f|J_0|\psi_i^\lambda\rangle| < |\langle\psi_f|J_0|\psi_i\rangle|. \qquad (39)$$

The above relation holds for most combinations of m_{J_d} and m_{s_f}. For those m_{J_d} and m_{s_f} for which Eq. (39) does

not hold, the absolute value of the matrix element is much smaller than for those for which the Eq. (39) *does* hold, and therefore we have f_L calculated from $\langle\psi_f|J_0|\psi_i^\lambda\rangle$ smaller than the f_L calculated from $\langle\psi_f|J_0|\psi_i\rangle$, as seen in Figs. 6 and 7.

b. Evolving the final state As indicated in Eq. (26), evolving the final state entails the evolution of the t-matrix. The overlap matrix element therefore is

$$\langle\psi_f^\lambda|J_0|\psi_i\rangle = \langle\phi|J_0|\psi_i\rangle + \langle\phi|t_\lambda^\dagger\,G_0^\dagger\,J_0|\psi_i\rangle. \qquad (40)$$

The IA term is the same as in the unevolved case. The SRG evolution leaves the on-shell part of the t-matrix—which is directly related to observables—invariant. The magnitude of the relevant off-shell t-matrix elements decreases on evolution, though. As a result we have

$$|\langle\psi_f^\lambda|J_0|\psi_i\rangle| < |\langle\psi_f|J_0|\psi_i\rangle|. \qquad (41)$$

This is reflected in f_L as calculated from the evolved final state, and seen in Figs. 6 and 7.

The effect of evolution of the initial state and the final state is to suppress f_L. When all the three components are evolved, we reproduce the unevolved answer as indicated in Fig. 6 and 7. It is therefore required that we find a huge enhancement when just the current is evolved.

The kinematics $E' = 30$ MeV, $\mathbf{q}^2 = 25$ fm^{-2} is further away from the quasi-free ridge than $E' = 30$ MeV, $\mathbf{q}^2 = 16$ fm^{-2}. The effects due to evolution discussed above get progressively more prominent the further away one is from the quasi-free ridge. This can be verified by comparing the effects due to evolution of individual components in Figs. 6 and 7.

As remarked earlier, away from the quasi-free ridge the FSI become important. Nonetheless, it is still instructive to look at f_L calculated in the IA at these kinematics.
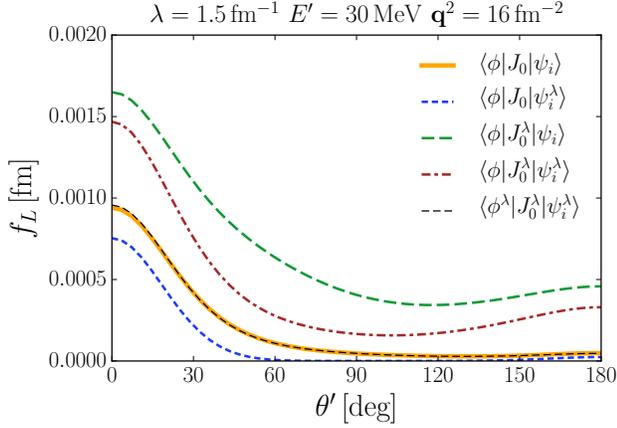
Figure 9. (color online) f_L in IA ($\langle\psi_f| \equiv \langle\phi|$) calculated for $E' = 30$ MeV and $\mathbf{q}^2 = 16$ fm^{-2} for the AV18 potential. Legends indicate which component of the matrix element in Eq. (30) used to calculate f_L are evolved.

Figure 10. (color online) f_L in IA ($\langle\psi_f| \equiv \langle\phi|$) calculated for $E' = 30$ MeV and $\mathbf{q}^2 = 25$ fm^{-2} for the AV18 potential. Legends indicate which component of the matrix element in Eq. (30) used to calculate f_L are evolved.
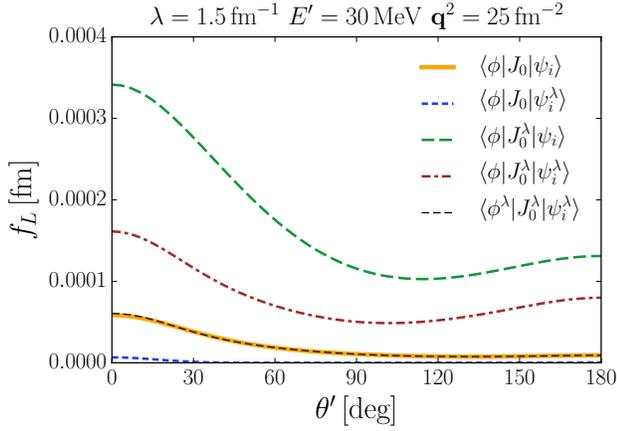
Note that the (unevolved) f_L calculated in the IA, shown in Figs. 9 and 10, is smaller than the full f_L that takes into account the final state interactions (*cf.* the corresponding curves in Figs. 6 and 7). This is consistent with the claim made earlier that below the quasi-free ridge the two terms in Eq. (13) add constructively.

The results in Figs. 9 and 10 can again be qualitatively explained based on our discussion above. The evolution of the deuteron wave function leads to suppression as the evolved wave function does not have strength at high momentum. The evolved current thus leads to enhancement. Evolution of both the current and the initial state decreases f_L from just the evolved current value, but it is not until we evolve all three components—final state, current, and the initial state—that we recover the unevolved answer.
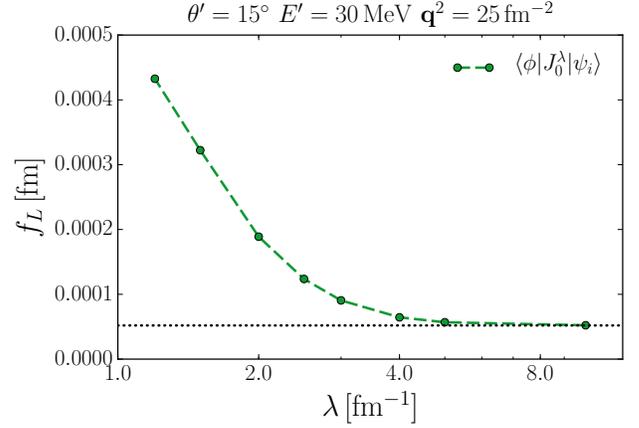

Figure 11. (color online) f_L in IA calculated at $\theta' = 15°$ for $E' = 30$ MeV and $\mathbf{q}^2 = 25$ fm^{-2} for the AV18 potential when the current operator in Eq. (30) used to calculate f_L is evolved to various SRG λ's. The horizontal dotted line is the unevolved answer.

As expected, the effect due to evolution increases with further evolution. This is illustrated in Fig. 11, where we investigate the effects of the current-operator evolution on f_L as a function of the SRG λ. To isolate the effect of operator evolution, we only look at f_L calculated in IA at a specific angle in Fig. 11.

4. Above the quasi-free ridge

Finally, we look at an example from above the quasi-free ridge. Figure 12 shows the effect of evolution of individual components on f_L for $E' = 100$ MeV and $\mathbf{q}^2 = 0.5$ fm^{-2}, which is point "4" in Fig. 3. The effects of evolution in this case are qualitatively different from those found below the quasi-free ridge. For instance, we see a peculiar suppression in f_L calculated from the evolved deuteron wave function at small angles, but an enhancement at large angles. An opposite behavior is observed for the final state. It is again possible to qualitatively explain these findings.

a. Evolving the initial state Above the quasi-free ridge, the IA and FSI terms in Eq. (13) add destructively. This can be seen by comparing the unevolved f_L curves in Figs. 12 and 13. Including the FSI brings down the value of f_L when one is above the quasi-free ridge.

At small angles, the magnitude of the IA term in Eq. (13) is larger than that of the FSI term. The deuteron wave function for this kinematics is probed between 1.2 and 1.9 fm^{-1}. With the wave-function evolution, the magnitude of the IA term in Eq. (38) decreases, whereas the magnitude of the FSI term in that equation slightly increases compared to its unevolved counterpart. Still, at small angles, we have $|\langle\phi|J_0|\psi_i^\lambda\rangle| > |\langle\phi|t^\dagger\, G_0^\dagger\, J_0|\psi_i^\lambda\rangle|$,
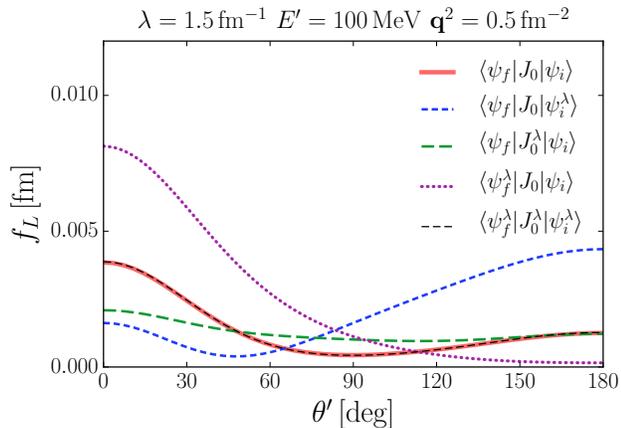
Figure 12. (color online) f_L calculated for $E' = 100$ MeV and $\mathbf{q}^2 = 0.5$ fm^{-2} (point "4" in Fig. 3) for the AV18 potential. Legends indicate which component of the matrix element in Eq. (30) used to calculate f_L is evolved. Opposite effects from the evolution of the initial state and the final state.

which leads to

$$|\langle\psi_f|J_0|\psi_i^\lambda\rangle| < |\langle\psi_f|J_0|\psi_i\rangle|, \qquad (42)$$

and thus to the suppression of f_L at small angles observed in Fig. 12.

At large angles, the magnitude of the IA term in Eq. (13) is smaller than that of the FSI term. With the wave-function evolution, the magnitude of IA term decreases substantially (large momenta in the deuteron wave function are probed at large angles, *cf.* Eq. (7)), whereas the FSI term in Eq. (13) remains almost the same. This results in increasing the difference between the two terms in Eq. (13) as the SRG λ is decreased. As mentioned before, above the quasi-free ridge, the IA and FSI terms in Eq. (13) add destructively and we therefore end up with $|\langle\psi_f|J_0|\psi_i^\lambda\rangle| > |\langle\psi_f|J_0|\psi_i\rangle|$, leading to the observed enhancement at large angles upon evolution of the wave function (see Fig. 12).

b. Evolving the final state The expression to consider is Eq. (40). With the evolution of the t-matrix, the magnitude of the term $\langle\phi|t_\lambda^\dagger G_0^\dagger J_0|\psi_i\rangle$ decreases, and because of the opposite relative signs of the two terms in Eq. (40)—and due to the fact that at small angles the magnitude of the IA term is larger than the FSI term— the net effect is $|\langle\psi_f^\lambda|J_0|\psi_i\rangle| > |\langle\psi_f|J_0|\psi_i\rangle|$. This leads to an enhancement of f_L with evolved final state at small angles, as seen in Fig. 12.

At large angles the magnitude of the IA term in Eq. (40) is smaller than that of the FSI term. With the evolution of the t-matrix, the magnitude of the FSI term decreases and the difference between the IA and the FSI terms decreases as well. This leads to the observed overall suppression in f_L at large angles due to the evolution of the final state seen in Fig. 12. For those few (m_{s_f}, m_{J_d}) combinations for which the above general observa-

tions do not hold, the value of individual components is too small to make any qualitative difference.
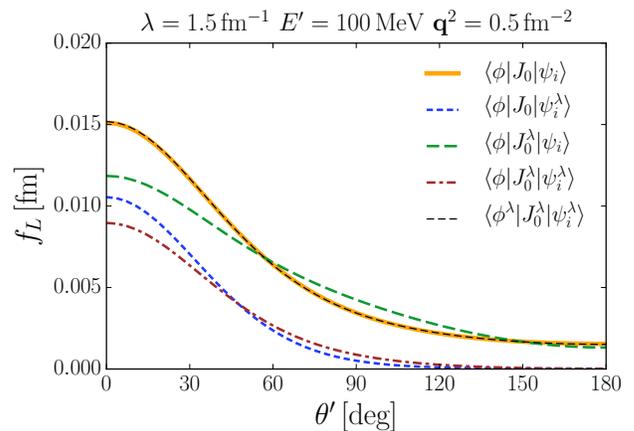

Figure 13. (color online) f_L in IA ($\langle\psi_f| \equiv \langle\phi|$) calculated for $E' = 100$ MeV and $\mathbf{q}^2 = 0.5$ fm^{-2} for the AV18 potential. Legends indicate which component of the matrix element in Eq. (30) used to calculate f_L are evolved.

Figure 13 shows the effect of evolution of individual components on f_L calculated in the IA for the kinematics under consideration. Again the evolved deuteron wave function does not have strength at high momenta and therefore f_L calculated from $\langle\phi|J_0|\psi_i^\lambda\rangle$ has a lower value than its unevolved counterpart.

Unitary evolution means that the effect of the evolved current is always such that it compensates the effect due to the evolution of the initial and final states. In future work we will examine more directly the behavior of the current as it evolves to better understand how to carry over the results observed here to other reactions.

IV. SUMMARY AND OUTLOOK

Nuclear properties such as momentum distributions are extracted from experiment by invoking the factorization of structure, which includes descriptions of initial and final states, and reaction, which includes the description of the probe components. The factorization between reaction and structure depends on the scale and scheme chosen for doing calculations. Unlike in high-energy QCD, this scale and scheme dependence of factorization is often not taken into account in low-energy nuclear physics calculations, but is potentially critical for interpreting experiment. In our work we investigated this issue by looking at the simplest knockout reaction: deuteron electrodisintegration. We used SRG transformations to test the sensitivity of the longitudinal structure function f_L to evolution of its individual components: initial state, final state, and the current.

We find that the effects of evolution depend on kinematics, but in a *systematic* way. Evolution effects are

negligible at the quasi-free ridge, indicating that the scale dependence of individual components is minimal there. This is consistent with the quasi-free ridge mainly probing the long-range part of the wave function, which is largely invariant under SRG evolution. This is also the region where contributions from FSI to f_L are minimal. The effects due to evolution get progressively more pronounced the further one moves away from the quasi-free ridge. The nature of changes due to evolution depends on whether one is above or below the quasi-free ridge in the 'phase-space' plot (Fig. 3). As indicated in Sec. III C, these changes can also be explained qualitatively by looking at the overlap matrix elements. This allows us to predict the effect due to evolution depending on kinematics.

Our results demonstrate that scale dependence needs to be taken into account for low-energy nuclear calculations. While we showed this explicitly only for the case of the longitudinal structure function in deuteron disintegration, we expect the results should qualitatively carry over for other knock-out reactions as well. An area of active investigation is the extension of the formalism presented here to hard scattering processes.

SRG transformations are routinely used in nuclear structure calculations because they lead to accelerated convergence for observables like binding energies. We demonstrated that SRG transformations can be used for nuclear knock-out reactions as well as long as the operator involved is also consistently evolved. The evolved operator appears to be complicated compared to the unevolved one, but the factorization might be cleaner with the evolved operator if one can exploit an operator product expansion [4, 33]. We plan to explore this in our future work.

We also plan to use pionless EFT as a framework to quantitatively study the effects of operator evolution. It should be a good starting point to understand in detail how a one-body operator develops strength in two- and higher-body sectors upon evolution. This can give insight on the issue of power counting of operator evolution. Pionless EFT has been employed previously to study deuteron electrodisintegration in Ref. [53], where it was used to resolve a discrepancy between theory and experiment.

Extending our work to many-body nuclei requires inclusion of 3N forces and 3N currents. Consistent evolution in that case would entail evolution in both two and three-body sectors. However, SRG transformations have proven to be technically feasible for evolving three-body forces [26–29]. Thus, extending our calculations to many-body nuclei would be computationally intensive, but is feasible in the existing framework. Including the effects of FSI is challenging for many-body systems and has been possible only recently for light nuclei [50, 54]. It would be interesting to investigate if the scale and scheme dependence of factorization allows us to choose a scale where the FSI effects are minimal.

ACKNOWLEDGMENTS

Appendix A: Expressions from evolution

Here we document the expressions used in Sec. II C. As seen in Eq. (23), in order to evaluate the term $\langle\phi|\,J_0^\lambda|\psi_i^\lambda\rangle$ we split it into four terms: B_1, B_2, B_3, and B_4. B_4 is obtained from Eq. (7) by using the evolved deuteron wave function instead of the unevolved one. The expressions for the terms B_3, B_2, and B_1 are as follows:

$$B_3 \equiv \langle\phi|\,J_0\,\widetilde{U}^\dagger|\psi_i^\lambda\rangle = 2\sqrt{\frac{2}{\pi}}\sum_{T_1=0,1}\left(G_E^p+(-1)^{T_1}\,G_E^n\right)\sum_{L_1=0}^{L_{\max}}\left(1+(-1)^{T_1}(-1)^{L_1}\right)Y_{L_1,m_{J_d}-m_{s_f}}(\theta',\varphi')$$

$$\times\sum_{J_1=|L_1-1|}^{L+1}\langle L_1\,m_{J_d}-m_{s_f}\,S=1\,m_{s_f}|J_1\,m_{J_d}\rangle\sum_{\widetilde{m}_s=-1}^{1}\langle J_1\,m_{J_d}|L_1\,m_{J_d}-\widetilde{m}_s\,S=1\,\widetilde{m}_s\rangle$$

$$\times\sum_{L_2=0}^{L_{\max}}\langle L_2\,m_{J_d}-\widetilde{m}_s\,S=1\,\widetilde{m}_s|J=1\,m_{J_d}\rangle\sum_{L_d=0,2}\int dk_3\,\psi_{L_d}^\lambda(k_3)\,k_3^2\int d\cos\theta\,P_{L_1}^{m_{J_d}-\widetilde{m}_s}(\cos\theta)$$

$$\times P_{L_2}^{m_{J_d}-\widetilde{m}_s}\!\left(\cos\alpha'(p',\theta)\right)\widetilde{U}\!\left(k_3,\sqrt{p'^2-p'q\cos\theta+q^2/4},L_d,L_2,J=1,S=1,T=0\right),\quad\text{(A1)}$$

$$B_2 \equiv \langle \phi | \, \widetilde{U} \, J_0 \, | \psi_i^\lambda \rangle = 2 \sqrt{\frac{2}{\pi}} \sum_{T_1 = 0,1} \left(G_E^p + (-1)^{T_1} G_E^n \right) \sum_{L_1 = 0}^{L_{\max}} \left(1 + (-1)^{T_1} (-1)^{L_1} \right) Y_{L_1, m_{J_d} - m_{s_f}}(\theta', \varphi')$$

$$\times \sum_{J_1 = |L_1 - 1|}^{L+1} \langle L_1 \, m_{J_d} - m_{s_f} \, S = 1 \, m_{s_f} | J_1 \, m_{J_d} \rangle \sum_{L_2, \widetilde{m}_s} \langle J_1 \, m_{J_d} | L_2 \, m_{J_d} - \widetilde{m}_s \, S = 1 \, \widetilde{m}_s \rangle$$

$$\times \sum_{L_d = 0,2} \langle L_d \, m_{J_d} - \widetilde{m}_s \, S = 1 \, \widetilde{m}_s | J = 1 \, m_{J_d} \rangle \int \mathrm{d}k_2 \, k_2^2 \, \widetilde{U}(p', k_2, L_1, L_2, J_1, S = 1, T_1)$$

$$\times \int \mathrm{d}\cos\theta \, P_{L_2}^{m_{J_d} - \widetilde{m}_s}(\cos\theta) \, P_{L_d}^{m_{J_d} - \widetilde{m}_s} \left(\cos\alpha'(k_2, \theta) \right) \psi_{L_d}^\lambda \left(\sqrt{k_2^2 - k_2 q \cos\theta + q^2/4} \right) , \quad \text{(A2)}$$

$$B_1 \equiv \langle \phi | \, \widetilde{U} \, J_0 \, \widetilde{U}^\dagger | \psi_i^\lambda \rangle = \frac{4}{\pi} \sqrt{\frac{2}{\pi}} \sum_{T_1 = 0,1} \left(G_E^p + (-1)^{T_1} G_E^n \right) \sum_{L_1 = 0}^{L_{\max}} \left(1 + (-1)^{T_1} (-1)^{L_1} \right) Y_{L_1, m_{J_d} - m_{s_f}}(\theta', \varphi')$$

$$\times \sum_{J_1 = |L_1 - 1|}^{L+1} \langle L_1 \, m_{J_d} - m_{s_f} \, S = 1 \, m_{s_f} | J_1 \, m_{J_d} \rangle \sum_{L_2, \widetilde{m}_s} \langle J_1 \, m_{J_d} | L_2 \, m_{J_d} - \widetilde{m}_s \, S = 1 \, \widetilde{m}_s \rangle$$

$$\times \sum_{L_3 = 0}^{L_{\max}} \langle L_3 \, m_{J_d} - \widetilde{m}_s \, S = 1 \, \widetilde{m}_s | J = 1 \, m_{J_d} \rangle \int \mathrm{d}k_2 \, k_2^2 \, \widetilde{U}(p', k_2, L_1, L_2, J_1, S = 1, T_1) \sum_{L_d = 0,2} \int \mathrm{d}k_4 \, k_4^2 \, \psi_{L_d}^\lambda(k_4)$$

$$\times \int \mathrm{d}\cos\theta \, P_{L_2}^{m_{J_d} - \widetilde{m}_s}(\cos\theta) \, P_{L_3}^{m_{J_d} - \widetilde{m}_s} \left(\cos\alpha'(k_2, \theta) \right) \widetilde{U} \left(k_4, \sqrt{k_2^2 - k_2 q \cos\theta + q^2/4}, L_d, L_3, J = 1, S = 1, T = 0 \right) .$$
$$\text{(A3)}$$

In deriving the equations for B_1, B_2, and B_3 we have made use of the fact that the matrix elements with J_0 are twice the matrix elements with J_0^-, $i.e.$, $\langle \phi | J_0 \, \widetilde{U}^\dagger | \psi_i^\lambda \rangle = 2 \langle \phi | J_0^- \, \widetilde{U}^\dagger | \psi_i^\lambda \rangle$, and similarly for B_2 and B_1 (cf. Sec. II B).

Evaluating Eq. (24) involves calculating the individual terms A_1, A_2, A_3, and A_4. The expressions for A_4 and A_3 can be obtained from expressions for B_2 and B_1, respectively, by replacing $\widetilde{U}$ with $\widetilde{U}^\dagger$. The U-matrices are real. Therefore, $\widetilde{U}^\dagger$ is obtained from $\widetilde{U}$ by interchanging momentum and angular momentum indices. The expressions for A_2 and A_1 are

$$A_2 \equiv \langle \phi | \widetilde{U}^\dagger \, \widetilde{U} \, J_0 | \psi_i^\lambda \rangle = \frac{4}{\pi} \sqrt{\frac{2}{\pi}} \sum_{T_1 = 0,1} \left(G_E^p + (-1)^{T_1} G_E^n \right) \sum_{L_1 = 0}^{L_{\max}} \left(1 + (-1)^{T_1} (-1)^{L_1} \right) Y_{L_1, m_{J_d} - m_{s_f}}(\theta', \varphi')$$

$$\times \sum_{J_1 = |L_1 - 1|}^{L+1} \langle L_1 \, m_{J_d} - m_{s_f} \, S = 1 \, m_{s_f} | J_1 \, m_{J_d} \rangle \sum_{L_3, \widetilde{m}_s} \langle J_1 \, m_{J_d} | L_3 \, m_{J_d} - \widetilde{m}_s \, S = 1 \, \widetilde{m}_s \rangle$$

$$\times \sum_{L_2 = 0}^{L_{\max}} \int \mathrm{d}k_2 \, k_2^2 \, \widetilde{U}(k_2, p', L_2, L_1, J_1, S = 1, T_1) \sum_{L_d = 0,2} \langle L_d \, m_{J_d} - \widetilde{m}_s \, S = 1 \, \widetilde{m}_s | J = 1 \, m_{J_d} \rangle$$

$$\times \int \mathrm{d}k_3 \, k_3^2 \, \widetilde{U}(k_2, k_3, L_2, L_3, J_1, S = 1, T_1) \int \mathrm{d}\cos\theta \, P_{L_3}^{m_{J_d} - \widetilde{m}_s}(\cos\theta)$$

$$\times P_{L_d}^{m_{J_d} - \widetilde{m}_s} \left(\cos\alpha'(k_3, \theta) \right) \psi_{L_d}^\lambda \left(\sqrt{k_3^2 - k_3 q \cos\theta + q^2/4} \right) \quad \text{(A4)}$$

and

$$
A_1 \equiv \langle \phi | \widetilde{U}^\dagger \, \widetilde{U} \, J_0 | \psi_i^\lambda \rangle = \frac{8}{\pi^2} \sqrt{\frac{2}{\pi}} \sum_{T_1=0,1} \left(G_E^p + (-1)^{T_1} G_E^n \right) \sum_{L_1=0}^{L_{\max}} \left(1 + (-1)^{T_1} (-1)^{L_1} \right) Y_{L_1, m_{J_d} - m_{s_f}}(\theta', \varphi')
$$

$$
\times \sum_{J_1 = |L_1 - 1|}^{L+1} \langle L_1 \, m_{J_d} - m_{s_f} \, S = 1 \, m_{s_f} | J_1 \, m_{J_d} \rangle \sum_{L_3, \widetilde{m}_s} \langle J_1 \, m_{J_d} | L_3 \, m_{J_d} - \widetilde{m}_s \, S = 1 \, \widetilde{m}_s \rangle
$$

$$
\times \sum_{L_4=0}^{L_{\max}} \langle L_4 \, m_{J_d} - \widetilde{m}_s \, S = 1 \, \widetilde{m}_s | J = 1 \, m_{J_d} \rangle \sum_{L_2=0}^{L_{\max}} \int dk_2 \, k_2^2 \, \widetilde{U}(k_2, p', L_2, L_1, J_1, S = 1, T_1)
$$

$$
\times \int dk_3 \, k_3^2 \, \widetilde{U}(k_2, k_3, L_2, L_3, J_1, S = 1, T_1) \sum_{L_d = 0,2} \int dk_5 \, k_5^2 \, \psi_{L_d}^\lambda(k_5) \int d\cos\theta \, P_{L_3}^{m_{J_d} - \widetilde{m}_s}(\cos\theta)
$$

$$
\times P_{L_4}^{m_{J_d} - \widetilde{m}_s}\left(\cos\alpha'(k_3, \theta) \right) \widetilde{U}\left(k_5, \sqrt{{k_3}^2 - k_3 q \cos\theta + q^2/4}, L_d, L_4, J = 1, S = 1, T = 0 \right) . \quad \text{(A5)}
$$

Evaluating the evolved current while including the final-state interactions involves computing the terms F_1, F_2, F_3, and F_4, as indicated in Eq. (28). F_4 is obtained from Eqs. (19) and (20) by replacing the deuteron wave function and the t-matrix by their evolved counterparts. The expressions for the terms F_3, F_2, and F_1 are then as follows:

$$
F_3 \equiv \langle \phi | t_\lambda^\dagger \, G_0^\dagger \, J_0 \, \widetilde{U}^\dagger | \psi_i^\lambda \rangle = \frac{4}{\pi} \sqrt{\frac{2}{\pi}} \frac{M}{\hbar c} \int \frac{dk_2 \, k_2^2}{(p' + k_2)(p' - k_2 - i\epsilon)} \sum_{T_1=0,1} \left(G_E^p + (-1)^{T_1} G_E^n \right) \sum_{L_1=0}^{L_{\max}} \left(1 + (-1)^{T_1} (-1)^{L_1} \right)
$$

$$
\times Y_{L_1, m_{J_d} - m_{s_f}}(\theta', \varphi') \sum_{J_1 = |L_1 - 1|}^{L+1} \langle L_1 \, m_{J_d} - m_{s_f} \, S = 1 \, m_{s_f} | J_1 \, m_{J_d} \rangle \sum_{L_2=0}^{L_{\max}} t_\lambda^*(k_2, p', L_2, L_1, J_1, S = 1, T_1)
$$

$$
\times \sum_{\widetilde{m}_s = -1}^{1} \langle J_1 \, m_{J_d} | L_2 \, m_{J_d} - \widetilde{m}_s \, S = 1 \, \widetilde{m}_s \rangle \sum_{L_3=0}^{L_{\max}} \langle L_3 \, m_{J_d} - \widetilde{m}_s \, S = 1 \, \widetilde{m}_s | J = 1 \, m_{J_d} \rangle \int d\cos\theta \, P_{L_2}^{m_{J_d} - \widetilde{m}_s}(\cos\theta)
$$

$$
\times P_{L_3}^{m_{J_d} - \widetilde{m}_s}\left(\cos\alpha'(k_2, \theta) \right) \int dk_5 \, k_5^2 \sum_{L_d = 0,2} \widetilde{U}\left(k_5, \sqrt{{k_2}^2 - k_2 q \cos\theta + q^2/4}, L_d, L_3, J = 1, S = 1, T = 0 \right) \psi_{L_d}^\lambda(k_5),
$$

$$
\text{(A6)}
$$

$$
F_2 \equiv \langle \phi | t_\lambda^\dagger \, G_0^\dagger \, \widetilde{U} \, J_0 | \psi_i^\lambda \rangle = \frac{4}{\pi} \sqrt{\frac{2}{\pi}} \frac{M}{\hbar c} \int \frac{dk_2 \, k_2^2}{(p' + k_2)(p' - k_2 - i\epsilon)} \sum_{T_1=0,1} \left(G_E^p + (-1)^{T_1} G_E^n \right) \sum_{L_1=0}^{L_{\max}} \left(1 + (-1)^{T_1} (-1)^{L_1} \right)
$$

$$
\times Y_{L_1, m_{J_d} - m_{s_f}}(\theta', \varphi') \sum_{J_1 = |L_1 - 1|}^{L+1} \langle L_1 \, m_{J_d} - m_{s_f} \, S = 1 \, m_{s_f} | J_1 \, m_{J_d} \rangle \sum_{L_2=0}^{L_{\max}} t_\lambda^*(k_2, p', L_2, L_1, J_1, S = 1, T_1)
$$

$$
\times \sum_{L_3=0}^{L_{\max}} \int dk_4 \, k_4^2 \, \widetilde{U}(k_2, k_4, L_2, L_3, J_1, S = 1, T_1) \sum_{\widetilde{m}_s = -1}^{1} \langle J_1 \, m_{J_d} | L_3 \, m_{J_d} - \widetilde{m}_s \, S = 1 \, \widetilde{m}_s \rangle
$$

$$
\times \sum_{L_d = 0,2} \langle L_d \, m_{J_d} - \widetilde{m}_s \, S = 1 \, \widetilde{m}_s | J = 1 \, m_{J_d} \rangle \int d\cos\theta \, P_{L_3}^{m_{J_d} - \widetilde{m}_s}(\cos\theta)
$$

$$
\times P_{L_d}^{m_{J_d} - \widetilde{m}_s}\left(\cos\alpha'(k_4, \theta) \right) \psi_{L_d}^\lambda\left(\sqrt{{k_4}^2 - k_4 q \cos\theta + q^2/4} \right) , \quad \text{(A7)}
$$

$$F_1 \equiv \langle \phi | t_\lambda^\dagger \, G_0^\dagger \, \widetilde{U} \, J_0 \, \widetilde{U}^\dagger | \psi_i^\lambda \rangle = \frac{8}{\pi^2} \sqrt{\frac{2}{\pi}} \frac{M}{\hbar c} \int \frac{\mathrm{d}k_2 \, k_2^2}{(p'+k_2)(p'-k_2-i\epsilon)} \sum_{T_1=0,1} \left(G_E^p + (-1)^{T_1} G_E^n \right) \sum_{L_1=0}^{L_{\max}} \left(1 + (-1)^{T_1}(-1)^{L_1} \right)$$

$$\times Y_{L_1, m_{J_d} - m_{s_f}}(\theta', \varphi') \sum_{J_1 = |L_1 - 1|}^{L+1} \langle L_1 \, m_{J_d} - m_{s_f} \, S = 1 \, m_{s_f} | J_1 \, m_{J_d} \rangle \sum_{L_2=0}^{L_{\max}} t_\lambda^*(k_2, p', L_2, L_1, J_1, S=1, T_1)$$

$$\times \sum_{L_3=0}^{L_{\max}} \sum_{\widetilde{m}_s = -1}^{1} \langle J_1 \, m_{J_d} | L_3 \, m_{J_d} - \widetilde{m}_s \, S = 1 \, \widetilde{m}_s \rangle \sum_{L_4=0}^{L_{\max}} \langle L_4 \, m_{J_d} - \widetilde{m}_s \, S = 1 \, \widetilde{m}_s | J = 1 \, m_{J_d} \rangle$$

$$\times \int \mathrm{d}k_4 \, k_4^2 \, \widetilde{U}(k_2, k_4, L_2, L_3, J_1, S=1, T_1) \int \mathrm{d}\cos\theta \, P_{L_3}^{m_{J_d} - \widetilde{m}_s}(\cos\theta) \, P_{L_4}^{m_{J_d} - \widetilde{m}_s}\left(\cos\alpha'(k_4, \theta) \right)$$

$$\times \int \mathrm{d}k_6 \, k_6^2 \sum_{L_d = 0,2} \widetilde{U}\left(k_6, \sqrt{{k_4}^2 - k_4 q \cos\theta + q^2/4}, L_d, L_4, J=1, S=1, T=0 \right) \psi_{L_d}^\lambda(k_6). \quad \text{(A8)}$$

Appendix B: Evolved final state

The interacting final neutron-proton state $|\psi_f\rangle$ as defined in Eq. (5) is the formal solution of the Lippmann–Schwinger (LS) equation for the scattering wave function,

$$\begin{aligned} |\psi_f\rangle &= |\phi\rangle + G_0(E') \, V |\psi_f\rangle \\ &= |\phi\rangle + G_0(E') \, t(E') |\phi\rangle . \end{aligned} \quad \text{(B1)}$$

The t-matrix, in turn, is defined by the LS equation

$$t(E') = V + V \, G_0(E') \, t(E') . \quad \text{(B2)}$$

The substitution $E' \to E' + i\epsilon$ and the limit $\epsilon \to 0$ are implied to select outgoing boundary conditions. We want to show now that the SRG-evolved final state can be obtained directly by using the solution t^λ of Eq. (B2) with $V \to V_\lambda$ in the second line of Eq. (B1), which is the same as Eq. (5) in Sec. II, i.e.,

$$U_\lambda |\psi_f\rangle = |\psi_f^\lambda\rangle , \quad \text{(B3)}$$

where

$$|\psi_f^\lambda\rangle = G_0(E') \, t_\lambda(E') |\phi\rangle . \quad \text{(B4)}$$

In this section, we suppress all spin and isospin degrees of freedom, and only denote the (arbitrary) energy parameter as E' for consistency with Sec. II.

First, it is important to recall that by definition the free Hamiltonian H_0 does not evolve, so that for $H = H_0 + V$ we have

$$H_\lambda = U_\lambda H \, U_\lambda^\dagger \equiv H_0 + V_\lambda . \quad \text{(B5)}$$

In other words, the evolved potential V_λ is defined such that it absorbs the evolution of the initial free Hamiltonian (kinetic energy) as well.

In order to prove Eq. (B3), it is convenient to consider the evolved and unevolved full Green's functions $G_\lambda(E')$ and $G(E')$, defined via

$$G_\lambda(z)^{-1} = z - H_\lambda = G_0^{-1}(z)^{-1} - V_\lambda , \quad \text{(B6a)}$$

$$G(z)^{-1} = z - H = G_0^{-1}(z)^{-1} - V . \quad \text{(B6b)}$$

Here, $G_0^{-1}(z)^{-1} = z - H_0$ is the free Green's function (which does not change under the SRG evolution because H_0 does not), and z is an arbitrary complex energy parameter that is set to $E' + i\epsilon$ to recover the physically relevant case. The Green's functions can be expressed in terms of the t-matrix as

$$G(z) = G_0(z) + G_0(z) \, t(z) \, G_0(z) , \quad \text{(B7)}$$

and analogously for the evolved version. Furthermore, the Green's functions can be written in their spectral representations

$$G_\lambda(z)^{-1} \simeq \int \mathrm{d}^3 k \, \frac{|\psi_f^\lambda(k)\rangle \langle \psi_f^\lambda(k)|}{z - k^2/M} + \text{bound states} , \quad \text{(B8a)}$$

$$G_\lambda(z)^{-1} \simeq \int \mathrm{d}^3 k \, \frac{|\psi_f(k)\rangle \langle \psi_f(k)|}{z - k^2/M} + \text{bound states} . \quad \text{(B8b)}$$

Here, $|\psi_f^{(\lambda)}(k)\rangle$ denotes the (evolved) continuum states with momentum k, and we have $|\psi_f^{(\lambda)}\rangle = |\psi_f^{(\lambda)}(\sqrt{ME'})\rangle$

From Eqs. (B5) and (B6) it now follows that

$$\begin{aligned} G_\lambda(z)^{-1} = z - H_\lambda &= z - U_\lambda H \, U_\lambda^\dagger \\ &= U_\lambda (z - H) U_\lambda^\dagger = U_\lambda \, G(z)^{-1} \, U_\lambda^\dagger . \quad \text{(B9)} \end{aligned}$$

Combining this with Eqs. (B8) and matching residues at $z = E' + i\epsilon$, we find that indeed $|\psi_f^\lambda\rangle = U_\lambda |\psi_f\rangle$, as stated in Eq. (B3).

[1] R. J. Furnstahl and K. Hebeler, Rept. Prog. Phys. **76**, 126301 (2013), arXiv:1305.3800 [nucl-th].

[2] S. K. Bogner, R. J. Furnstahl, and A. Schwenk, Prog. Part. Nucl. Phys. **65**, 94 (2010), arXiv:0912.3688 [nucl-th].

[3] R. J. Furnstahl and A. Schwenk, J. Phys. G **37**, 064005 (2010), arXiv:1001.0328 [nucl-th].

[4] E. Anderson, S. Bogner, R. Furnstahl, and R. Perry, Phys. Rev. C **82**, 054001 (2010), arXiv:1008.1569 [nucl-th].

[5] R. J. Furnstahl, in *Proceedings, International Conference on Nuclear Theory in the Supercomputing Era (NTSE-2013)* (2013) p. 371, arXiv:1309.5771 [nucl-th].

[6] L. Frankfurt, M. Sargsian, and M. Strikman, Int. J. Mod. Phys. A **23**, 2991 (2008), arXiv:0806.4412 [nucl-th].

[7] J. Arrington, D. Higinbotham, G. Rosner, and M. Sargsian, Prog. Part. Nucl. Phys. **67**, 898 (2012), arXiv:1104.1196 [nucl-ex].

[8] A. Rios, A. Polls, and W. H. Dickhoff, Phys. Rev. **C89**, 044303 (2014), arXiv:1312.7307 [nucl-th].

[9] W. Boeglin and M. Sargsian, Int. J. Mod. Phys. **E24**, 1530003 (2015), arXiv:1501.05377 [nucl-ex].

[10] W. P. Ford, S. Jeschonnek, and J. W. Van Orden, Phys. Rev. **C90**, 064006 (2014), arXiv:1411.3306 [nucl-th].

[11] F. Sammarruca, (2015), arXiv:1507.07043 [nucl-th].

[12] O. Hen, L. B. Weinstein, E. Piasetzky, G. A. Miller, and M. M. Sargsian, (2014), arXiv:1407.8175 [nucl-ex].

[13] R. Weiss, B. Bazak, and N. Barnea, Phys.Rev.Lett. **114**, 012501 (2015), arXiv:1405.2734 [nucl-th].

[14] R. Weiss, B. Bazak, and N. Barnea, (2015), arXiv:1503.07047 [nucl-th].

[15] S. Hoinka, M. Lingham, K. Fenech, H. Hu, C. J. Vale, J. E. Drut, and S. Gandolfi, Phys. Rev. Lett. **110**, 055305 (2013).

[16] T. Duguet, H. Hergert, J. D. Holt, and V. Somà, Phys. Rev. **C92**, 034313 (2015), arXiv:1411.1237 [nucl-th].

[17] E. Epelbaum, H.-W. Hammer, and U.-G. Meißner, Rev. Mod. Phys. **81**, 1773 (2009), arXiv:0811.1338 [nucl-th].

[18] H.-W. Hammer, A. Nogga, and A. Schwenk, Rev. Mod. Phys. **85**, 197 (2013), arXiv:1210.4273 [nucl-th].

[19] J. Carlson, S. Gandolfi, F. Pederiva, S. C. Pieper, R. Schiavilla, K. E. Schmidt, and R. B. Wiringa, (2014), 10.1103/RevModPhys.87.1067, arXiv:1412.3081 [nucl-th].

[20] L. E. Marcucci, F. Gross, M. T. Pena, M. Piarulli, R. Schiavilla, I. Sick, A. Stadler, J. W. Van Orden, and M. Viviani, (2015), arXiv:1504.05063 [nucl-th].

[21] S. Quaglioni, G. Hupin, A. Calci, P. Navratil, and R. Roth (2015) arXiv:1509.09009 [nucl-th].

[22] S. Bacca, N. Barnea, G. Hagen, G. Orlandini, and T. Papenbrock, Phys. Rev. Lett. **111**, 122502 (2013), arXiv:1303.7446 [nucl-th].

[23] M. Pine, D. Lee, and G. Rupak, Eur. Phys. J. **A49**, 151 (2013), arXiv:1309.2616 [nucl-th].

[24] M. D. Schuster, S. Quaglioni, C. W. Johnson, E. D. Jurgenson, and P. Navratil, Phys. Rev. **C90**, 011301 (2014), arXiv:1402.7106 [nucl-th].

[25] T. Neff, H. Feldmeier, and W. Horiuchi, Phys. Rev. **C92**, 024003 (2015), arXiv:1506.02237 [nucl-th].

[26] E. D. Jurgenson, P. Navratil, and R. J. Furnstahl, Phys. Rev. Lett. **103**, 082501 (2009), arXiv:0905.1873 [nucl-th].

[27] E. Jurgenson, P. Navratil, and R. Furnstahl, Phys. Rev.

[28] K. Hebeler, Phys. Rev. C **85**, 021002 (2012), arXiv:1201.0169 [nucl-th].

[29] K. A. Wendt, Phys. Rev. C **87**, 061001 (2013), arXiv:1304.1431 [nucl-th].

[30] S. Boffi, C. Giusti, F. D. Pacati, and M. Radici, *Electromagnetic Response of Atomic Nuclei* (Clarendon Press, Oxford, 1996).

[31] "White paper on nuclear astrophysics and low-energy nuclear physics," www.lecmeeting.org (January 2015).

[32] C. C. d. Atti, Phys. Rept. **590**, 1 (2015).

[33] S. Bogner and D. Roscher, Phys. Rev. C **86**, 064304 (2012), arXiv:1208.1734 [nucl-th].

[34] C.-J. Yang and D. R. Phillips, Eur. Phys. J. A **49**, 122 (2013), arXiv:1305.7279 [nucl-th].

[35] H. Arenhövel, W. Leidemann, and E. L. Tomusiak, Eur. Phys. J. **A23**, 147 (2005), arXiv:nucl-th/0407053 [nucl-th].

[36] S. Gilad, W. Bertozzi, and Z. L. Zhou, *Proceedings, 15th International IUPAP Conference on Few body problems in physics (FB15)*, Nucl. Phys. **A631**, 276 (1998).

[37] K. S. Egiyan *et al.* (CLAS), Phys. Rev. Lett. **98**, 262502 (2007), arXiv:nucl-ex/0701013 [nucl-ex].

[38] H. Arenhövel *et al.*, Z. Phys. A **331** (1988).

[39] W.-J. Kasdorp, *Deuteron electrodisintegration at large momentum values*, Ph.d thesis, Amsterdam (1966).

[40] H. Arenhövel, W. Leidemann, and E. L. Tomusiak, Phys. Rev. **C46**, 455 (1992).

[41] R. H. Landau, *Quantum Mechanics II* (John Wiley & Sons, New York, 1989).

[42] C.-J. Yang, *Subtractive Renormalization of the NN interaction in Chiral Effective Theory and the Deuteron Electro-disintegration Calculation*, Ph.d thesis, Ohio University (2010).

[43] J. H. Hetherington and L. H. Schick, Phys. Rev. **137**, B935 (1965).

[44] E. W. Schmid and H. Ziegelmann, *The Quantum Mechanical Three-Body Problem* (Vieweg, Braunschweig, 1974).

[45] S. Bochkanov, "ALGLIB," www.alglib.net (September 2015).

[46] Intel®, "Threading Building Blocks (TBB)," www.threadingbuildingblocks.org (September 2015).

[47] R. J. Furnstahl and H.-W. Hammer, Phys. Lett. B **531**, 203 (2002), nucl-th/0108069.

[48] R. B. Wiringa, V. G. J. Stoks, and R. Schiavilla, Phys. Rev. C **51**, 38 (1995), arXiv:nucl-th/9408016.

[49] J. Carlson and R. Schiavilla, Rev. Mod. Phys. **70**, 743 (1998).

[50] S. Bacca and S. Pastore, J. Phys. **G41**, 123002 (2014), arXiv:1407.3490 [nucl-th].

[51] R. Machleidt, Phys. Rev. C **63**, 024001 (2001), arXiv:nucl-th/0006014.

[52] D. R. Entem and R. Machleidt, Phys. Rev. C **68**, 041001 (2003), nucl-th/0304018.

[53] S. Christlmeier and H. W. Griesshammer, Phys. Rev. **C77**, 064001 (2008), arXiv:0803.1307 [nucl-th].

[54] A. Lovato, S. Gandolfi, J. Carlson, S. C. Pieper, and R. Schiavilla, Phys. Rev. **C91**, 062501 (2015), arXiv:1501.01981 [nucl-th].

C **83**, 034301 (2011), arXiv:1011.4085 [nucl-th].